Power Flow Decoupling Controller for Triple Active Bridge Based on Fourier Decomposition of Transformer Currents

Purgat, Pavel; Bandyopadhyay, Soumya; Qin, Zian; Bauer, Pavol

DOI
10.1109/APEC39645.2020.9124006

Publication date
2020

Document Version
Final published version

Published in
APEC 2020 - 35th Annual IEEE Applied Power Electronics Conference and Exposition

Power Flow Decoupling Controller for Triple Active Bridge Based on Fourier Decomposition of Transformer Currents

1st Pavel Purgat
Electrical Sustainable Energy
TU Delft
Delft, The Netherlands
p.purgat@tudelft.nl

2nd Soumya Bandyopadhyay
Electrical Sustainable Energy
TU Delft
Delft, The Netherlands
s.bandopathay-2@tudelft.nl

3rd Zian Qin
Electrical Sustainable Energy
TU Delft
Delft, The Netherlands
z.qin-2@tudelft.nl

4th Pavol Bauer
Electrical Sustainable Energy
TU Delft
Delft, The Netherlands
p.bauer@tudelft.nl

***Abstract*—This paper proposes a power flows decoupling controller for the triple active bridge converter. The controller is based on a full-order continuous-time model of the TAB converter derived using the generalized average modelling (GAM) technique. GAM uses the Fourier series expansion to decompose the state-space variables into two components, which represent the active power and the reactive power. The controller uses the active power components of the transformer currents to decouple the active power flows between converter ports. Additionally, the implementation of the decoupling controller in the digital domain is detailed in the paper. The decoupling performance of the proposed controller is validated in a hardware experiment.**

***Index Terms*—control, decoupling, dc microgrid, Fourier series, power flow control**

I. Introduction

In recent years, multi-port converters (MPC) have gained research attention as a potential solution for versatile energy management systems able to integrate diverse renewable energy sources or conventional energy sources, storage systems, and loads [1]. The main advantages of MPCs include lower component count compared to standalone converters, higher efficiency, the possibility of centralized control, and potentially higher power density. Potential applications for the MPCs range from electric vehicles [2], more-electric aircrafts [3], [4] to smart grids [5], [6].

The primary purpose of multi-port converters (MPC) is to integrate multiple sources, storages, and loads with varied voltage and current ratings into a single power stage allowing bi-directional power flow between each port. Apart from bi-directional power flow, specific applications like EV charging also require galvanic isolation between the different ports for safety reasons [7]. Hence, a multi-winding high-frequency (HF) transformer is used. One of the promising topologies in the multi-winding transformer-coupled MPC family is the triple-active bridge (TAB) converter. The TAB converter is an MPC with three inverter bridges (half-bridge or full-bridge) connected via a high frequency (HF) multi-winding transformer [7], [8]. Derived from the dual-active bridge (DAB) converter family [9], the TAB converter not only integrates and exchanges the energy from/to all ports, but also provides full isolation among all ports and matches the different port voltage levels. Additionally, the TAB converter can operate with soft-switching conditions across a broad operating range [10].

A key challenge of TAB converter design and control is the inherent cross-coupling of the power flows between the ports due to the multi-winding transformer. Therefore, the TAB converter behaves as a multi-input multi-output (MIMO) system with coupled control loops. In literature, three control techniques to decouple the power flows are reported. A feedforward compensator based control method is proposed in [11], which decouples the control loops dynamically with pre-calculated gains stored as a look-up table in the controller. This approach is improved with feedforward control in [12] or reformulated using conjugated variables in [13]. Another control technique decouples the control loops by choosing different bandwidths for the single-input single-output (SISO) loops [14]. Therefore, the loop with the highest bandwidth determines the phase-shift direction during transients and acts as the slack bus. Recently, a time-sharing control is reported in [8], which decouples the power flows by operating the MAB converter as a DAB converter with only two active ports and other ports deactivated as diode rectifiers at any particular period. Currently, all approaches to decouple the control variables are based on the first order simplified model [15]-[16].

The main contribution of this paper is the derivation and the experimental verification of the active power decoupling controller for the phase-shifted TAB. The controller is derived, and its implementation in the digital domain is proposed. The proposed controller is validated by an experimental study on a TAB laboratory prototype. The rest of this paper is organized as follows. Section II recapitulates GAM and explains the state-space model of the TAB converter. In section III, the active current based decoupling controller is proposed. The implementation of the proposed controller in the digital domain is explained in section IV. Section IV further provides experimental verification of the proposed controller. Section V summarizes the paper and provides an outlook on future work.

978-1-7281-4829-8/20/$31.00 ©2020 IEEE

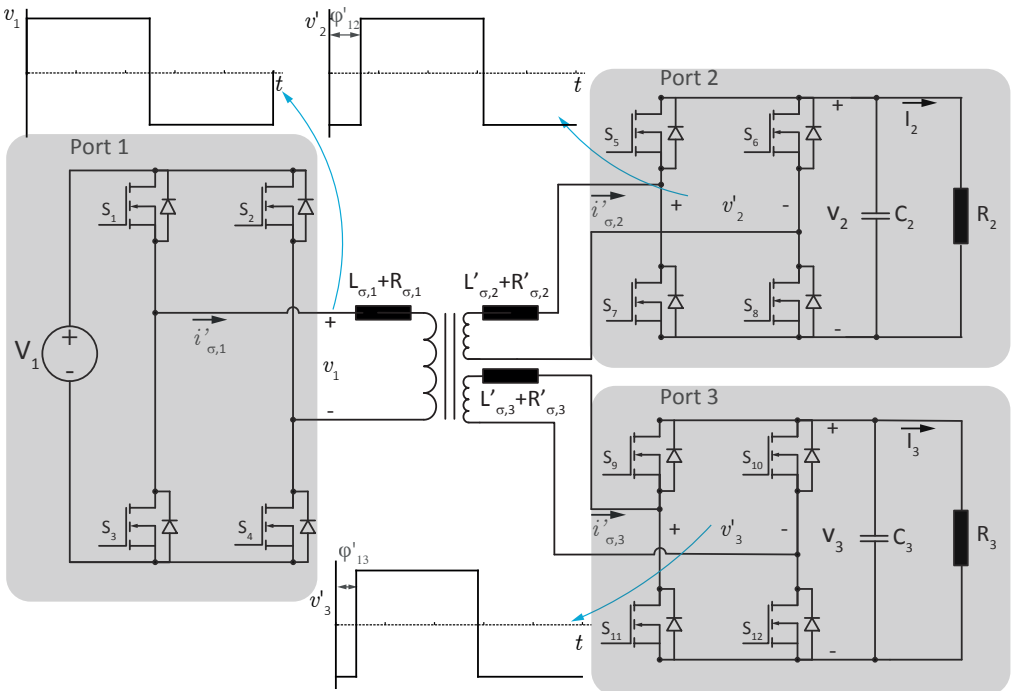

Fig. 1: Triple active bridge converter.

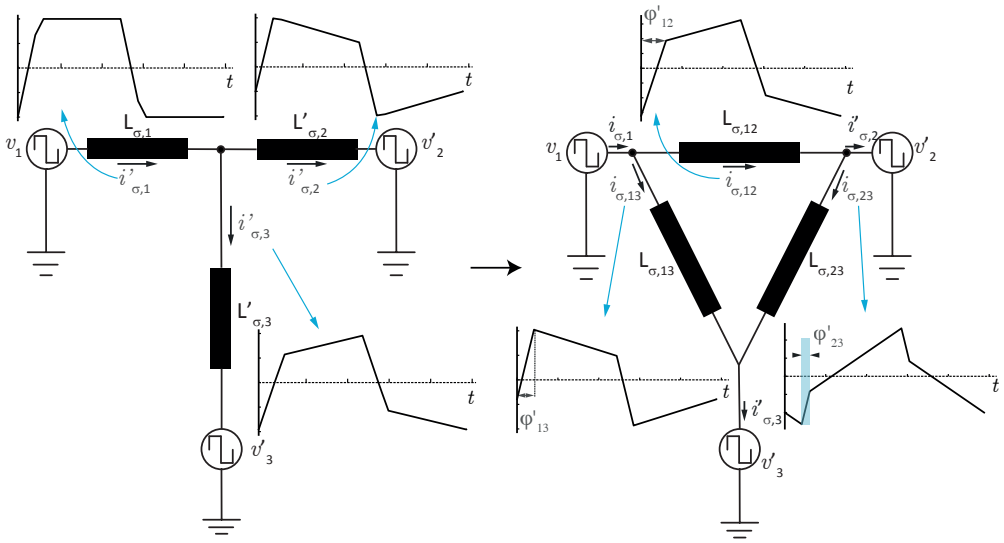

Fig. 2: Simplified schematic of TAB in star and delta connection.

II. Operation & Modelling Principles

Triple active bridge (TAB) converter is derived from the dual active bridge (DAB) converter family. Figure 1 shows the schematic of the TAB converter. The TAB converter consists of three ac generating cells connected to a transformer with three windings. The power is transferred across the leakage inductances that can be inserted as separate components, or the transformer leakage inductances can be used. The zero-voltage switching (ZVS) is achieved utilizing the parasitic capacitance of full bridges MOSFETs.

The equation derived for the DAB cycle-by-cycle average (CCA) power in [9] can be extended to a TAB converter. Thus, the CCA power transferred (P_{ij}) from port j into port k of a TAB converter is given by

$$P_{\mathrm{ij}} = \frac{V_i^{'} V_j^{'}}{2\pi f_s L_{\sigma,\mathrm{ij}}} \varphi_{\mathrm{ij}} \left(1 - \frac{|\varphi_{\mathrm{ij}}|}{\pi}\right), \qquad \varphi_{\mathrm{ij}} = \varphi_{\mathrm{i}} - \varphi_{\mathrm{j}}, \quad (1)$$

where $L_{\sigma,\mathrm{ij}}$ is the equivalent inductance between ports i and j, φ_{i} and φ_{j} are the corresponding phase shift angles, $V_i^{'}$ and $V_j^{'}$ are the corresponding dc port voltages. Therefore, the

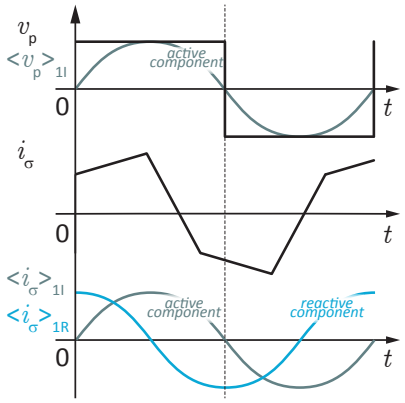

Fig. 3: Active and circulating power components.

power flow at each port of TAB converter can be controlled in three ways: (a) phase-shift (φ_{ij}) control between the full bridges, (b) duty-cycle control of the full bridges, and (c) switching frequency (f_s) control. This paper focuses only on the phase shift control. For the phase-shift control, the duty cycle on the full bridges is kept at 50%, and the power transfer is controlled by the phase shifts between the full bridges. To analyze the power transfer between the ports, the equivalent inductance between the ports needs to computed/estimated. Therefore, it is beneficial to convert the schematic in Fig. 1 into a delta equivalent circuit.

The transformation from star to delta equivalent circuit of the TAB converter is shown in Fig. 2. The transformer is described as a Δ connection. The current waveforms of the converter are shown in Fig. 2. As was done in [7], the link inductances in Δ connection can be computed based on the individual leakage inductances of the transformer windings

$$L_{\sigma,12} = L_{\sigma,1} + N^2 L_{\sigma,2} + \frac{L_{\sigma,1}L_{\sigma,2}}{L_{\sigma,3}}, \tag{2}$$

$$L_{\sigma,13} = L_{\sigma,1} + N^2 L_{\sigma,3} + \frac{L_{\sigma,1}L_{\sigma,3}}{L_{\sigma,2}}, \tag{3}$$

$$L_{\sigma,32} = N^2 L_{\sigma,3} + N^2 L_{\sigma,2} + N^4 \frac{L_{\sigma,3}L_{\sigma,2}}{L_{\sigma,1}}, \tag{4}$$

where N is the transformer ratio and $L_{\sigma,1}$, $L_{\sigma,2}$ and $L_{\sigma,3}$ are the transformer leakage inductances and the transformer ratio is accounted as $L'_{\sigma,2} = N^2 L_{\sigma,2}$ and $L'_{\sigma,3} = N^2 L_{\sigma,3}$. Similarly, the transformer currents of the TAB converter after transformation are

$$i_{\sigma,1} = -i_{\sigma,12} - i_{\sigma,13}, \tag{5}$$

$$i'_{\sigma,2} = i_{\sigma,12} - i_{\sigma,23}, \tag{6}$$

$$i'_{\sigma,3} = i_{\sigma,13} + i_{\sigma,23}, \tag{7}$$

where $i_{\sigma,1}$ is the primary side transformer current and $i'_{\sigma,2}$ and $i'_{\sigma,3}$ are the secondary side transformer currents. The transformer ratio is accounted as $i'_{\sigma,2} = N i_{\sigma,2}$ and $i'_{\sigma,3} = N i_{\sigma,3}$.

A. Generalized Average Modelling

The generalized averaging method (GAM) was derived in [17], motivated by the switching circuits that did not fulfill the small-ripple condition. MPC that are derived from DAB fall into this category; therefore, when the transformer harmonics are to be captured, GAM must be applied. The generalized averaging method was applied to the DAB in [18]. GAM rotates around the fact that any waveform $x(t)$ can be represented to arbitrary accuracy by a Fourier series on a given interval $t - T_s \leq \tau < t$. For periodic signals, this property can be represented as

$$x(\tau) = \sum_{l=-\infty}^{\infty} \langle x \rangle_l(t) e^{-jl\omega_s \tau}, \tag{9}$$

where $\omega_s = 2\pi f_s$, the sum is over all integers l and $\langle x \rangle_l$ is the $l-th$ coefficient of the Fourier series. These coefficients are functions of time and can be expressed as

$$\begin{aligned} \langle x \rangle_l(t) &= \frac{1}{T}\int_{t-T+s}^{t} x(\tau) e^{-jl\omega_s\tau} \mathrm{d}\tau \\ &= \frac{1}{T}\int_{t-T+s}^{t} x(\tau)\cos(l\omega_s\tau)\mathrm{d}\tau \\ &\quad - \frac{j}{T}\int_{t-T+s}^{t} x(\tau)\sin(l\omega_s\tau)\mathrm{d}\tau. \end{aligned} \tag{10}$$

In eq. (10) the *sine* component is in phase with the ac voltage and it is the active power component while the *cosine* component represents the reactive power as shown in Fig. 3. This convention is adopted here to keep the derived equations in line with the preceding works [17]–[19].

B. Large Signal Model

The equations describing the operation of TAB converter using delta convention shown in Fig.**??** are

$$C_2 \frac{\mathrm{d}}{\mathrm{d}\tau} v_2(\tau) = -\frac{v_2(\tau)}{R_2} + s_2(\tau) i'_{\sigma,2}(\tau), \tag{11}$$

$$C_3 \frac{\mathrm{d}}{\mathrm{d}\tau} v_3(\tau) = -\frac{v_3(\tau)}{R_3} + s_3(\tau) i'_{\sigma,3}(\tau), \tag{12}$$

$$L_{\sigma,12}\frac{\mathrm{d}}{\mathrm{d}\tau} i_{\sigma,12}(\tau) = -R_{\sigma,12} i_{\sigma,12}(\tau) + v_1(\tau) - v'_2(\tau), \tag{13}$$

$$L_{\sigma,13}\frac{\mathrm{d}}{\mathrm{d}\tau} i_{\sigma,13}(\tau) = -R_{\sigma,13} i_{\sigma,13}(\tau) + v_1(\tau) - v'_3(\tau), \tag{14}$$

$$L_{\sigma,23}\frac{\mathrm{d}}{\mathrm{d}\tau} i_{\sigma,23}(\tau) = -R_{\sigma,23} i_{\sigma,23}(\tau) + v'_2(\tau) - v'_3(\tau), \tag{15}$$

where C_2, C_3 are the output capacitances, R_2 and R_3 are the output resistances and $R_{\sigma,12}$, $R_{\sigma,13}$ and $R_{\sigma,23}$ are the parasitic resistances in the delta type equivalent circuit of the TAB, transformed the same way as the leakage inductances.

In (11)(15), it is assumed that the transformer magnetization current is insignificant. Further, the MOSFET switching transients are neglected as well as the voltage drop across the MOSFET body diode. The input capacitance is coupled in the ideal voltage source V_1, and the reason is twofold. First, the input capacitance is normally large enough to minimize any

$$\frac{\mathrm{d}}{\mathrm{d}t}\begin{bmatrix} V_2 \\ V_3 \\ i_{\sigma,12R} \\ i_{\sigma,12I} \\ i_{\sigma,13R} \\ i_{\sigma,13I} \\ i_{\sigma,23R} \\ i_{\sigma,23I} \end{bmatrix} = \begin{bmatrix} \frac{-1}{R_2C_2} & 0 & \frac{-4N\sin(d_1\pi)}{\pi C_2} & \frac{-4N\cos(d_1\pi)}{\pi C_2} & 0 & 0 & \frac{4N\sin(d_1\pi)}{\pi C_2} & \frac{4N\cos(d_1\pi)}{\pi C_2} \\ 0 & \frac{-1}{R_3C_3} & 0 & 0 & \frac{-4N\sin(d_2\pi)}{\pi C_3} & \frac{-4N\cos(d_2\pi)}{\pi C_3} & -\frac{4N\sin(d_2\pi)}{\pi C_3} & -\frac{4N\cos(d_2\pi)}{\pi C_3} \\ \frac{2N\sin(d\pi)}{\pi L_{\sigma,12}} & 0 & \frac{-R_{\sigma,12}}{L_{\sigma,12}} & \omega_s & 0 & 0 & 0 & 0 \\ \frac{2N\cos(d\pi)}{\pi L_{\sigma,12}} & 0 & -\omega_s & \frac{-R_{\sigma,12}}{L_{\sigma,12}} & 0 & 0 & 0 & 0 \\ 0 & \frac{2N\sin(d_2\pi)}{\pi L_{\sigma,13}} & 0 & 0 & \frac{-R_{\sigma,13}}{L_{\sigma,13}} & \omega_s & 0 & 0 \\ 0 & \frac{2N\cos(d_2\pi)}{\pi L_{\sigma,13}} & 0 & 0 & -\omega_s & \frac{-R_{\sigma,13}}{L_{\sigma,13}} & 0 & 0 \\ \frac{2N\sin(d_1\pi)}{\pi L_{\sigma,23}} & \frac{-2N\sin(d_2\pi)}{\pi L_{\sigma,23}} & 0 & 0 & 0 & 0 & \frac{-R_{\sigma,23}}{L_{\sigma,23}} & \omega_s \\ \frac{-2N\cos(d_1\pi)}{\pi L_{\sigma,23}} & \frac{2N\cos(d_2\pi)}{\pi L_{\sigma,23}} & 0 & 0 & 0 & 0 & -\omega_s & \frac{-R_{\sigma,23}}{L_{\sigma,23}} \end{bmatrix}$$
$$\times \begin{bmatrix} V_2 \\ V_3 \\ i_{\sigma,12R} \\ i_{\sigma,12I} \\ i_{\sigma,13R} \\ i_{\sigma,13I} \\ i_{\sigma,23R} \\ i_{\sigma,23I} \end{bmatrix} + \begin{bmatrix} 0 \\ 0 \\ 0 \\ \frac{-2}{\pi L_{\sigma,12}} \\ 0 \\ \frac{-2}{\pi L_{\sigma,13}} \\ 0 \\ 0 \end{bmatrix} \left[V_{\text{in}}\right]. \tag{8}$$

voltage ripple. Secondly, in most applications, it is desired to control the voltages on the secondary side of the converter; therefore, output capacitors C_2 and C_3 and their respective dynamics are modeled. The parasitic resistances $R_{\sigma,12}$, $R_{\sigma,13}$ and $R_{\sigma,23}$ represent both the ohmic losses in the magnetic circuit as well as in the semiconductors. The large-signal model can be derived by applying GAM (10) on the converter model in (11)-(15). Further, it is assumed that the dynamics of the input voltage source and the voltages on the output capacitors C_2 and C_3 are much slower than that of the TAB transformer. Therefore the capacitor voltages $V_2(\tau)$ and $V_3(\tau)$ are described only by the zero-order component of the Fourier series, while the inductor currents are described with the fundamental component i.e., the switching frequency component.

The generalized averaging method will not be applied explicitly here to eq. (11)-(15) as modeling is not the primary goal of this paper. However, the generalized averaging method was explicitly applied to TAB equations in [20]. The large-signal model of the TAB can be written in the state-space form, as shown in eq. (8).

III. Decoupling Controller

The instantaneous powers of the converter ports connected in delta convention shown in Fig. **??** can be written as

$$\begin{aligned} \langle P_{\text{p},1}\rangle_{1I}(t) &= \langle v_1\rangle_{1I}(t)\langle i_{\sigma,1}\rangle_{1I}(t) \\ &= \langle v_1\rangle_{1I}(t)\left(\langle i_{\sigma,12}\rangle_{1I}(t) + \langle i_{\sigma,13}\rangle_{1I}(t)\right), \end{aligned} \tag{16}$$

$$\begin{aligned} \langle P_{\text{p},2}\rangle_{1I}(t) &= \langle v_2\rangle_{1I}(t)\langle i_{\sigma,2}\rangle_{1I}(t) \\ &= \langle v_2\rangle_{1I}(t)\left(-\langle i_{\sigma,12}\rangle_{1I}(t) + \langle i_{\sigma,23}\rangle_{1I}(t)\right), \end{aligned} \tag{17}$$

$$\begin{aligned} \langle P_{\text{p},3}\rangle_{1I}(t) &= \langle v_3\rangle_{1I}(t)\langle i_{\sigma,3}\rangle_{1I}(t) \\ &= \langle v_3\rangle_{1I}(t)\left(-\langle i_{\sigma,13}\rangle_{1I}(t) - \langle i_{\sigma,23}\rangle_{1I}(t)\right), \end{aligned} \tag{18}$$

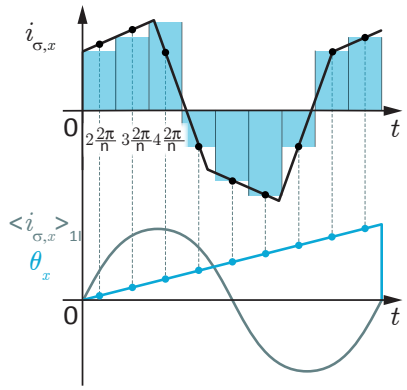

Fig. 4: Extraction of the active component of the measured variable in discrite time.

where $\langle x\rangle_{1I}(t)$ is the first coefficient in the Fourier series representing active power as shown in Fig. 3.

It is clear from eq. (18) that the port powers of TAB can be decoupled by compensating for the influence of the current $\langle i_{\sigma,23}\rangle_{1I}$ in the control loops of the ports two and three. In [19], a controller for DAB was proposed that uses the active power component of the transformer current. In [19] it was shown that using the active power component reduces the transient DC component, thereby reduces the peak flux density. The controller proposed in this work uses the active power components of the transformer currents extracted from the raw data and calculated in a DSP.

A. Active Current Component Extraction

In the derivation of the extraction of the active current component, it is assumed that the signals are periodic. The Fourier series coefficient corresponding to the active component in the

time domain can be written as

$$\langle x\rangle_k(t) = -\frac{1}{T_s}\int_{T_s} x(\tau)\sin(k\omega_s\tau)\mathrm{d}\tau. \tag{19}$$

The extraction of the active component is measured periodically n times across the switching period T_s. The integration is substituted by dividing the integration to intervals with defined length of $k\frac{T_s}{n}$. In period $\frac{T_s}{n} \leq \tau < (k+1)\frac{T_s}{n}$, the integrand $x(\tau)\sin(k\omega_s\tau)$ is approximated by $\tau = k\frac{T_s}{n}$ which means

$$x\left(k\frac{T_s}{n}\right)\sin\left(\frac{2\pi}{T_s}k\frac{T_s}{n}\right) = x\left(k\frac{T_s}{n}\right)\sin\left(\frac{2\pi}{n}k\right).$$

Therefore the integration over the specified period is approximated by the area of the rectangle with the height of $x\left(k\frac{T_s}{n}\right)\sin\left(\frac{2\pi}{n}k\right)$ and width of $\frac{T_s}{n}$. When the rectangle area is substituted to (19) then the discrete approximation can be written as

$$\langle x\rangle_k(t) \approx \langle x\rangle_k^{(n)} = -\frac{1}{T_s}\sum_{k=0}^{n-1}\frac{T_s}{n}x\left(\frac{T_s}{n}k\right)\sin\left(\frac{2\pi}{n}k\right) = \tag{20}$$

$$-\frac{1}{n}\sum_{k=0}^{n-1}x\left(\frac{T_s}{n}k\right)\sin\left(\frac{2\pi}{n}k\right). \tag{21}$$

Equation (21) can be rewritten in the form corresponding with the one shown in [19] if the PWM carrier period $\theta_x = \frac{2\pi}{T_s}$ and $x[n-k] = x\left(\frac{T_s}{n}k\right)$, then it can be written

$$\langle i_{\sigma,x}\rangle_{1I}[n] = -\frac{1}{n}\sum_{k=0}^{n-1}\left(i_{\sigma,x}\left[n-k\right]\sin\left(\theta_x\left[n-k\right]\right)\right), \tag{22}$$

where the x in θ_x and $i_{\sigma,x}$ denotes the number of the corresponding full-bridge in the TAB. This is because the extraction of the fundamental component of the ac currents must be done at a position referred to the corresponding ac port voltage. Therefore, the extraction is synchronized via the reference angle θ_x, which is the carrier wave of the corresponding PWM, i.e., PWM 2 or PWM 3. Equation (22) is the complete expression describing the extraction of the active component. The timing diagram of the active power components extraction subroutine is shown in Fig. 4.

B. Coupling Current Estimation Using Transformer Voltages

To apply the proposed decoupling control, current $i_{\sigma,23}(t)$ needs to be estimated. The current between the ports two and three is given by the voltage difference across the inductor $L_{\sigma,23}$. When $R_{\sigma,23}$ is assumed to be negligible, (15) can be written as

$$L_{\sigma,23}\frac{\mathrm{d}}{\mathrm{d}\tau}i_{\sigma,23}(\tau) = v_2'(\tau) - v_3'(\tau). \tag{23}$$

In integral form (23) can be written as

$$i_{\sigma,23}(t) = \frac{1}{L_{\sigma,23}}\int_{t_1}^{t_2} v_2'(\tau) - v_3'(\tau)\mathrm{d}\tau. \tag{24}$$

Using the trapezoidal rule, (24) can be estimated as

$$i_{\sigma,23}(t) = \frac{1}{L_{\sigma,23}}\int_{t_1}^{t_2} v_2'(\tau) - v_3'(\tau)\mathrm{d}\tau \tag{25}$$

$$\approx \frac{t_2-t_1}{2L_{\sigma,23}}\left(v_2'(t_2) - v_3'(t_2) + v_2'(t_1) - v_3'(t_1)\right). \tag{26}$$

Equation (26) can be rewritten in terms of sampling speed f_n and written as

$$i_{\sigma,23}[n] = \frac{f_n}{2L_{\sigma,23}}\left(\Delta v'[n] + \Delta v'[n-1]\right), \tag{27}$$

where $\Delta v'[n] = v_2'(t_2) - v_3'(t_2)$ and $\Delta v'[n-1] = v_2'(t_1) - v_3'(t_1)$. Extraction of the active component can be easily performed combining (27) and (22) obtaining

$$\langle i_{\sigma,23}\rangle_{1I}^{(\theta_2)}[n] = -\frac{1}{n}\sum_{k=0}^{n-1} i_{\sigma,23}[n-k]\sin\left(\theta_2\left[n-k\right]\right), \tag{28}$$

$$\langle i_{\sigma,23}\rangle_{1I}^{(\theta_3)}[n] = -\frac{1}{n}\sum_{k=0}^{n-1} i_{\sigma,23}[n-k]\sin\left(\theta_3\left[n-k\right]\right), \tag{29}$$

for port two and port three, respectively. Result of (28) and (29) can be used as the decoupling current for their respective ports as explained at the beginning of this section and described with (17)-(18).

C. Coupling Current Estimation Using DC Capacitor Voltages

The disadvantage of the method derived in the previous subsection is the measurement of the high-frequency voltages. These voltages have different potentials, and the measurements must be galvanically isolated. If isolated amplifiers are used to measure these voltages, the induced delays by the measurements are $1\mu s$ to $3\mu s$. These delays can be significant, especially when the phase angles are small.

The large-signal model matrix offers a solution to avoid the measurement of the high-frequency voltages. The equations describing the coupling current $i_{\sigma,23}$ can be rewritten in integral form as

$$\langle i_{\sigma,23}\rangle_{1R} = \int_{t_1}^{t_2}\frac{2n\sin(d_1\pi)V_2}{\pi L_{\sigma,23}} - \frac{2n\sin(d_2\pi)V_3}{\pi L_{\sigma,23}} - \frac{R_{\sigma,23}\langle i_{\sigma,23}\rangle_{1R}}{L_{\sigma,23}} + \omega_s\langle i_{\sigma,23}\rangle_{1I}\quad \mathrm{d}t, \tag{30}$$

$$\langle i_{\sigma,23}\rangle_{1I} = \int_{t_1}^{t_2} -\frac{2n\cos(d_1\pi)V_2}{\pi L_{\sigma,23}} + \frac{2n\cos(d_2\pi)V_3}{\pi L_{\sigma,23}} - \frac{R_{\sigma,23}\langle i_{\sigma,23}\rangle_{1I}}{L_{\sigma,23}} - \omega_s\langle i_{\sigma,23}\rangle_{1R}\quad \mathrm{d}t. \tag{31}$$

Using trapezoidal rule (30)-(31) can be rewritten for the

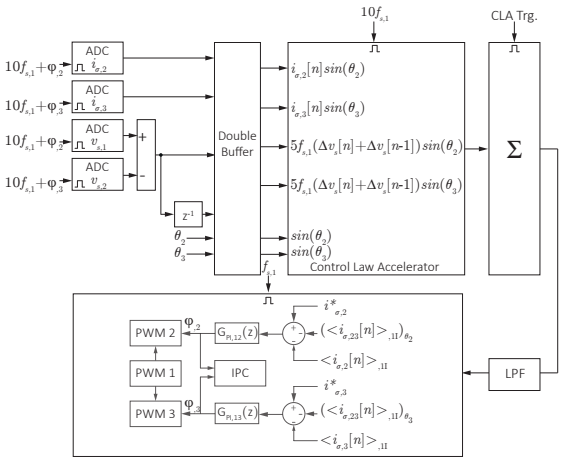

Fig. 5: Proposed implementaion of the decoupling controller in the digital domain.

discrete domain as

$$\begin{aligned}\langle i_{\sigma,23}\rangle_{1R}[n] \approx \frac{f_n}{2L_{\sigma,23}}\Big(&\\ \frac{2N}{\pi}\left(\sin(d_1[n]\pi)V_2[n]-\sin(d_1[n-1]\pi)V_2[n-1]\right)&\\ -\frac{2N}{\pi}\left(\sin(d_2[n]\pi)V_3[n]-\sin(d_2[n-1]\pi)V_3[n-1]\right)&\\ -R_{\sigma,23}\left(\langle i_{\sigma,23}\rangle_{1R}[n]-\langle i_{\sigma,23}\rangle_{1R}[n-1]\right)&\\ +\frac{\omega_s}{L_{\sigma,23}}\left(\langle i_{\sigma,23}\rangle_{1I}[n]-\langle i_{\sigma,23}\rangle_{1I}[n-1]\right)\Big),&\end{aligned} \tag{32}$$

and

$$\begin{aligned}\langle i_{\sigma,23}\rangle_{1I}[n] \approx \frac{f_n}{2L_{\sigma,23}}\Big(&\\ \frac{2N}{\pi}\left(\cos(d_1[n]\pi)V_2[n]-\cos(d_1[n-1]\pi)V_2[n-1]\right)&\\ -\frac{2N}{\pi}\left(\cos(d_2[n]\pi)V_3[n]-\cos(d_2[n-1]\pi)V_3[n-1]\right)&\\ -R_{\sigma,23}\left(\langle i_{\sigma,23}\rangle_{1I}[n]-\langle i_{\sigma,23}\rangle_{1I}[n-1]\right)&\\ -\frac{\omega_s}{L_{\sigma,23}}\left(\langle i_{\sigma,23}\rangle_{1R}[n]-\langle i_{\sigma,23}\rangle_{1R}[n-1]\right)\Big).&\end{aligned} \tag{33}$$

Result of (33) can be used as the decoupling current as explain at the beginning of this section and described in equations (17)-(18).

IV. Implementation & Experiment

A. Controller Implementation

The overall structure of the proposed controller and its implementation in the digital domain is shown in Fig. 5. The controller is implemented on *TMS320F28379D* digital signal processor (DSP). The used DSP is equipped with an independent 32-bit floating-point math processor referred to as Control Law Accelerator (CLA) [21]. CLA helps with concurrent-loop execution and is capable of reading ADC samples just after ADC finishes reading. Therefore CLA is used to implement time-critical mathematical tasks, i.e., extraction of the active current component. The used DSP is equipped with two CPUs. CPU 1 implements the controller and sends control signals over the inter-processor communication (IPC) link to CPU 2. CPU 2 communicates with the laboratory computer.

The secondary transformer currents and secondary transformer voltages are sampled ten times per switching period. The sampling of currents and voltages is synchronized with the respective PWMs as shown by $(10f_{s,1}+\varphi_x)$ in Fig. 5. The ADC signals are scaled and sent via a double buffer to CLA. The double buffer is necessary as the CLA task is executed asynchronously with the CPU clock. The CLA also receives the time base periods θ_2 and θ_3 of PWM 2 and PWM 3. The time base periods of the respective PWMs are used to calculate the corresponding trigonometric functions for active component extraction. Inside the CLA, sines of the two driving periods, θ_2 and θ_3 are calculated as well as the multiplication of different signals, as shown in Fig. 3. After completion of each CLA task, a buffer is triggered. The results of the CLA task are read, and the summation of the results is performed once per switching period in a separate task on CPU 1. In every period, a controller subroutine is called. In the controller subroutine, the calculated active components of currents are used to close the loop, and corresponding phase-shifts are calculated with PI controllers. The phase-shifts are communicated via IPC to CPU 2.

The ADCs measuring currents and voltages are triggered ten times faster than the driving PWMs - PWM1, PWM2, and PWM 3. The ADCs are synchronized with PWM 2, and PWM 3 and correspondingly phase shifted with respect to PWM 1. From the measured raw data, the active power components are extracted as described in Fig. 4 and further fed to the PI blocks that regulate the converter operation as shown in Fig. 5.

TABLE I: Prototype Parameters

Parameter	Acronym	Value
Transformer ratio	N	7 [-]
Primary Inductance	$L_{\sigma,1}$	70 [μH]
Secondary Inductance	$L_{\sigma,x}$	1.5 [μH]
Output Capacitance	$C_{\text{out,x},x}$	1.22 [mF]
Primary Resistance	$R_{\sigma,1}$	20 [mΩ]
Secondary Resistance	$R_{\sigma,x}$	.4 [mΩ]

B. Experiment

The operation of the proposed controller is verified in the hardware experiments. The prototype parameters are summarized in Table I. The converter switching frequency is 20 kHz. The load resistances R_2 and R_3 were 10Ω. The main goal of the experiment is to demonstrate the decoupling of the power flow P_{12} and P_{13} inside of the TAB converter. To this end, each port of the converter is stepped separately up and down. The results are shown in Fig. 6 and Fig. 7.

The response of the load currents to step in the reference of port two is shown in Fig. 6a. The load current $i_{\text{load},1}$ changes and tracks the reference. The load current I_3 is only slightly disturbed. The same step change is repeated with port three.

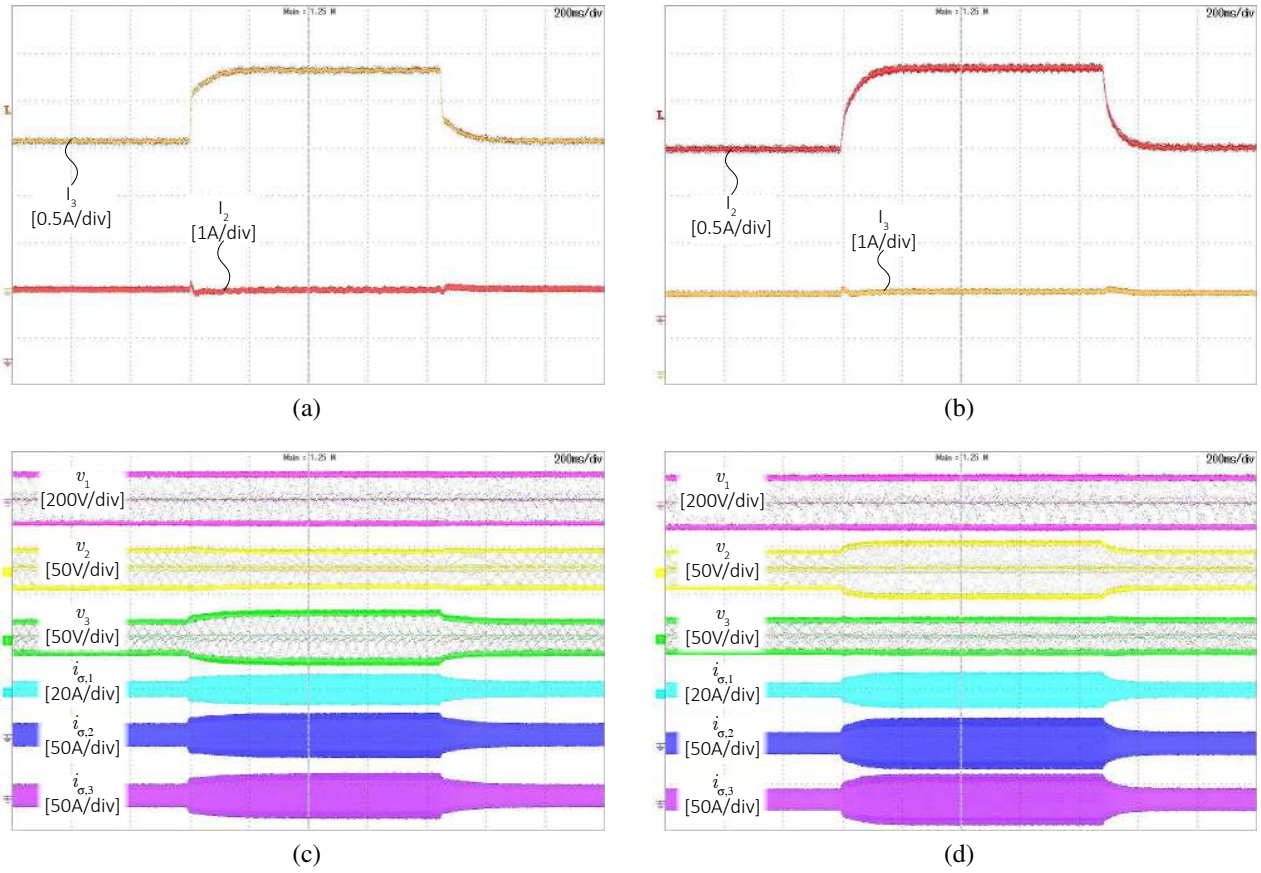

Fig. 6: Step response of the proposed controller using dc capacitor voltage based coupling estimator. In (a) are the load currents response to change in reference of $i^*_{\sigma,2}$, in (b) are the load currents response to change in reference of $i^*_{\sigma,3}$. In (c) and (d) are the transformer currents and voltages.

Figures 7b show similar performance and good disturbance rejection. The results show the operation of the controller when the dc capacitor voltages are used for coupling current estimation. The high-frequency signals during steps are shown in Fig. 6c and Fig. 6d showing smooth envelopes and good disturbance rejection on the transformer state-space variables as well.

The response of the load currents to step in the reference for ports two and three when the estimator based on the transformer voltages is used are shown in Fig. 7. As can be seen, the controller decouples the power flows very fast. Moreover, a faster step can be achieved when the PI controllers bandwidth is increased. The high-frequency signals during steps using the transformer voltage based estimator are shown in Fig. 7d and Fig. 7c showing smooth envelopes and good disturbance rejection on the transformer state-space variables as well.

V. Conclusion

In this paper, a new approach to the decoupling control of the triple active bridge (TAB) is derived and verified in hardware experiments. The fundamental difference between the proposed controller and the previous work is the use of the ac transformer current dynamics to achieve the decoupling of the control variables. The paper analyses the physical origin of the power flow coupling. A coupling current component is defined using the delta convention. Two estimators of the coupling current component are derived. The implementation of the decoupling controller in the digital domain is thoroughly analyzed and described.

References

[1] A. K. Bhattacharjee, N. Kutkut, and I. Batarseh, "Review of multiport converters for solar and energy storage integration," *IEEE Transactions on Power Electronics*, vol. 34, no. 2, pp. 1431–1445, 2018.

[2] S. Y. Kim, H. Song, and K. Nam, "Idling port isolation control of three-port bidirectional converter for evs," *IEEE Transactions on Power Electronics*, vol. 27, no. 5, pp. 2495–2506, May 2012.

[3] P. Wheeler and S. Bozhko, "The more electric aircraft: Technology and challenges." *IEEE Electrification Magazine*, vol. 2, pp. 6–12, 2014.

[4] G. Sulligoi, A. Vicenzutti, and R. Menis, "All-electric ship design: From electrical propulsion to integrated electrical and electronic power systems," *IEEE Transactions on Transportation Electrification*, 2016.

[5] M. Neubert, A. Gorodnichev, J. Gottschlich, and R. W. D. Doncker, "Performance Analysis of a Triple-Active Bridge Converter for Interconnection of Future DC-Grids," *2016 IEEE Energy Conversion Congress and Exposition*, pp. 1–8, 2016.

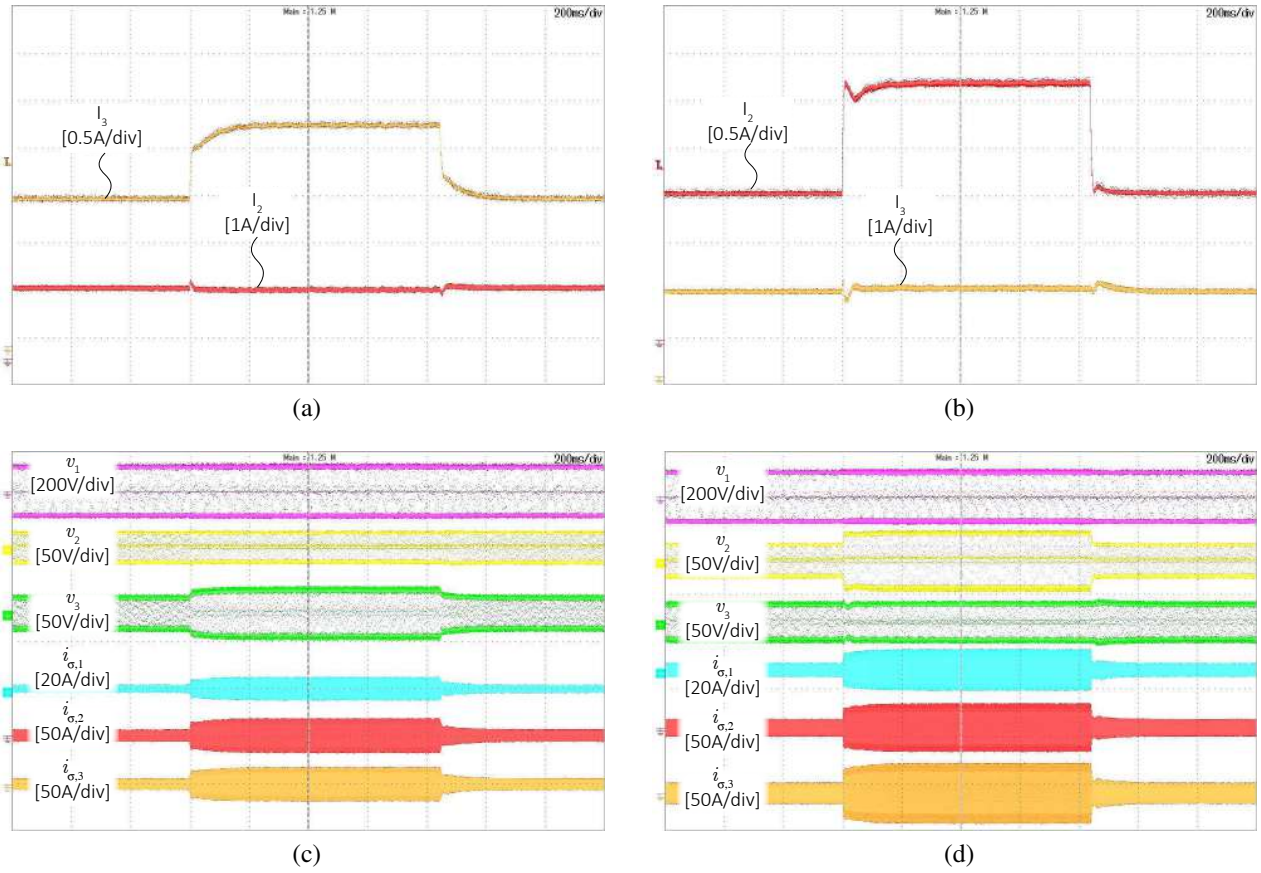

Fig. 7: Step response of the proposed controller using transformer voltage based coupling estimator. In (a) are the load currents response to change in reference of $i^*_{\sigma,2}$, in (b) are the load currents response to change in reference of $i^*_{\sigma,3}$. In (c) and (d) are the transformer currents and voltages.

[6] P. Purgat, L. Mackay, M. Schulz, Y. Han, Z. Qin, M. März, and P. Bauer, "Design of a power flow control converter for bipolar meshed lvdc distribution grids," in *2018 IEEE 18th International Power Electronics and Motion Control Conference*, Aug 2018, pp. 1073–1078.

[7] C. Zhao and J. W. Kolar, "A novel three-phase three-port ups employing a single high-frequency isolation transformer," in *Power Electronics Specialists Conference, 2004. PESC 04. 2004 IEEE 35th Annual*, vol. 6. IEEE, 2004, pp. 4135–4141.

[8] Y. Chen, P. Wang, H. Li, and M. Chen, "Power flow control in multi-active-bridge converters: Theories and applications," in *2019 IEEE Applied Power Electronics Conference and Exposition*. IEEE, 2019.

[9] R. W. De Doncker, D. M. Divan, and M. H. Kheraluwala, "A three-phase soft-switched high-power-density dc/dc converter for high-power applications," *IEEE transactions on industry applications*, vol. 27, no. 1, pp. 63–73, 1991.

[10] W. Jiang, Z. Zhang, X. Bie, and Z. Xu, "Operating area for modular multilevel converter based high-voltage direct current systems," *IET Renewable Power Generation*, vol. 10, no. 6, pp. 776–787, 2016. [Online]. Available: http://digital-library.theiet.org/content/journals/10.1049/iet-rpg.2015.0342

[11] C. Zhao, S. D. Round, and J. W. Kolar, "An isolated three-port bidirectional dc-dc converter with decoupled power flow management," *IEEE transactions on power electronics*, vol. 23, pp. 2443–2453, 2008.

[12] T. Ohno and N. Hoshi, "A new control method for triple-active bridge converter with feed forward control," in *2018 International Power Electronics Conference (IPEC-Niigata 2018 -ECCE Asia)*, May 2018, pp. 971–976.

[13] M. Grabarek, M. Parchomiuk, and R. Strzelecki, "Conjugated control of triple active bridge converter with common hft," in *2017 11th IEEE International Conference on Compatibility, Power Electronics and Power Engineering (CPE-POWERENG)*, April 2017, pp. 304–307.

[14] H. Tao, A. Kotsopoulos, J. Duarte, and M. Hendrix, "A soft-switched three-port bidirectional converter for fuel cell and supercapacitor applications," in *PESC'05. 36th*. IEEE, 2005, pp. 2487–2493.

[15] C. Zhao, S. D. Round, and J. W. Kolar, "An isolated three-port bidirectional dc-dc converter with decoupled power flow management," *IEEE Transactions on Power Electronics*, vol. 23, no. 5, pp. 2443–2453, Sept 2008.

[16] H. Tao, J. L. Duarte, and M. A. M. Hendrix, "Three-port triple-half-bridge bidirectional converter with zero-voltage switching," *IEEE Transactions on Power Electronics*, vol. 23, no. 2, pp. 782–792, March 2008.

[17] S. R. Sanders, J. M. Noworolski, X. Z. Liu, and G. C. Verghese, "Generalized averaging method for power conversion circuits," *IEEE Transactions on Power Electronics*, vol. 6, no. 2, pp. 251–259, April 1991.

[18] H. Qin and J. W. Kimball, "Generalized average modeling of dual active bridge dc–dc converter," *IEEE Transactions on Power Electronics*, vol. 27, no. 4, pp. 2078–2084, April 2012.

[19] S. S. Shah and S. Bhattacharya, "Control of active component of current in dual active bridge converter," in *2018 IEEE Applied Power Electronics Conference and Exposition (APEC)*, March 2018, pp. 323–330.

[20] P. Purgat, S. Bandyopadhyay, Z. Qin, and P. Bauer, "Continuous time full order model of triple active bridge converter," in *2019 21st European Conference on Power Electronics and Applications (EPE'19 ECCE Europe)*, Sep. 2019.

[21] *TMS320F2837xD-Technical Reference Manual*, Texas Instruments.